# Electrocatalytic Amplification of Nanoparticle Collisions at Electrodes Modified with Polyelectrolyte Multilayer Films

Alma D. Castañeda, Timothy M. Alligrant, James A. Loussaert, and Richard M. Crooks*

Department of Chemistry, Center for Electrochemistry, and the Center for Nano- and Molecular Science and Technology, The University of Texas at Austin, 105 East 24th Street, Stop A5300, Austin, Texas 78712-1224, United States

Ⓢ *Supporting Information*

ABSTRACT: We report electrochemical catalytic amplification of individual collisions between ~57 nm diameter Pt nanoparticles (Pt NPs) and 12.5 μm diameter Au ultramicroelectrodes modified with passivating, electrostatically assembled polyelectrolyte multilayer (PEM) films prepared by the layer-by-layer deposition method. Two key findings are reported. First, despite the thicknesses of the insulating PEM films, which range up to 5 nm, electrons are able to tunnel from the Pt NPs to the electrode resulting in electrocatalytic N_2H_4 oxidation at the PEM film−solution interface. These single-particle measurements are in accord with prior reports showing that the electrochemical activity of passive PEM films can be reactivated by adsorption of metallic NPs. Second, it is possible to control the frequency of the collisions by manipulating the net electrostatic charge present on the outer surface of the PEM thin film. These results, which demonstrate that chemistry can be used to control electrocatalytic amplification, set the stage for future sensing applications.
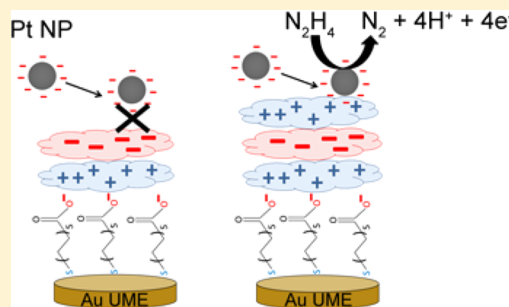
INTRODUCTION

We report electrochemical detection of collisions between individual Pt nanoparticles (Pt NPs) and Au ultramicroelectrodes (Au UMEs) modified with passivating polyelectrolyte multilayer (PEM) films prepared using the layer-by-layer deposition method.[1,2] Our results build on recent findings that individual collisions between NPs and naked electrode surfaces can be detected by electrocatalytic amplification (ECA).[3,4] The important new result reported here is that, in addition to naked electrode surfaces, these collisions can be detected through PEM films having thicknesses of up to ~5.3 nm, which is well beyond normal electron tunneling distance. Interestingly, electrocatalytic reactions between negatively charged Pt NPs and PEMs can be activated and deactivated by controlling the charge on the final layer of the film. Specifically, when the outermost layer is composed of cationic poly-L-lysine (pLL), current transients corresponding to collisions are observed, but when the charge is reversed by addition of a layer of poly-L-glutamic acid (pGA), current transients are effectively turned off. This observation of chemical control over collisions may provide a means for developing chemical sensors based on ECA.

ECA, first reported by Bard and co-workers,[3−13] is based on measuring redox reactions that occur selectively on electrocatalytically active NPs when they come into contact with a noncatalytic electrode surface. Here, we have chosen N_2H_4 oxidation (eq 1) as the redox reaction and an appropriately modified Au UME as the noncatalytic electrode. To ensure that the Au UME itself does not participate in electrooxidation of N_2H_4, its potential is set sufficiently negative so that the background current is low.

$$N_2H_4 = N_2 + 4H^+ + 4e^- \qquad (1)$$

Bard and co-workers found that when these experimental conditions are correctly configured, injection of Pt NPs into an electrolyte solution containing N_2H_4 results in current transients; each of these corresponds to a Pt NP striking the electrode surface. Moreover, it was found that the Pt NPs stick to the electrode surface, leading to step-shaped transients that slowly decay (the mechanism for this decay has not been definitively identified). In addition to the Au UME−Pt NP−N_2H_4 system, a number of other combinations of redox species (N_2H_4, BH_4^-, H_2O (oxidation), H_2O_2, and H^+), and electrode materials (C, Au, Pt, Pt−O) have been identified that yield signatures of collisions.[7] Moreover, the Compton group[14−21] has made important contributions to this field by reporting current transients arising from electrodissolution[14,15] and electrodeposition[16,18] of colliding NPs. The Stevenson group showed that Hg and Bi electrodes can be used for ECA experiments and that in the case of Hg, deactivation of the colliding NPs is very fast.[22] They observed the appearance of sharp spike-shaped current transients that presumably arise because of the rapid deactivation of Pt NPs by Hg. Additionally, the Alpuche-Aviles,[23] Andreescu,[24] Koper,[25,26] Macpherson,[27] Unwin,[25] and Zhang[12,28−30] groups have all made important contributions that have provided insights into this interesting phenomenon. Finally, we[31] and the Bard group[9] have begun to

apply the principles of ECA to chemical sensing, with an ultimate goal of detecting single DNA molecules and proteins.

To date, most ECA experiments have involved naked electrode surfaces, but chemically modified electrodes have also been examined. For example, Bard and co-workers[6] demonstrated that the amplitude of current transients arising from collisions is attenuated when a Au electrode is modified with a carboxyl-terminated *n*-alkylthiol self-assembled monolayer (SAM).[32] Specifically, they observed a negative logarithmic correlation between catalytic current and the number of carbons in the alkyl chain. For example, a 12-mercaptodecanoic acid-modified UME yielded current steps of just ~5 pA, which can be compared to a naked Au surface where current transients were on the order of ~60 pA. More recently, the Bard group also reported on collisions between Pt NPs and Pt UMEs modified with a thin, insulating film of TiO$_2$.[33]

The studies reported here were motivated by the work of the Allongue[34] and Fermín groups.[35] Specifically, the Fermín group used the LbL deposition method to prepare pinhole-free films containing pLL and pGA on Au electrodes.[36] These polymer layers were sufficiently thick that little or no electron transfer was observed between the electrode and a molecular redox probe in solution. However, when the surface of the film was modified with Au NPs, facile electron transfer was turned on even through films as thick as 6.5 nm. They interpreted this result in terms of the increased tunneling probability between the electrode and the high density of states of the adsorbed NPs (compared to that of molecules), as previously predicted by Allongue and co-workers.[34] These results have since been confirmed by other groups using a variety of intervening organic materials and conductive NPs.[37−41]

In the present work, we modified 12.5 μm diameter Au UMEs with an 11-mercaptoundecanoic acid (MUA) SAM, followed by immobilization of alternating layers of pLL (positively charged) and pGA (negatively charged) (Scheme 1). Because the citrate capping agent on the Pt NPs is deprotonated at pH 7, the NPs can be electrostatically adsorbed to films having a pLL terminating layer.[35] Accordingly, collisions between the Pt NPs and the polymer layer result in transients in current−time (*i*−*t*) traces for the SAM−pLL- and SAM−pLL−pGA−pLL-modified UMEs. In contrast, no

collisions resulting in significant current transients are observed on the SAM−pLL−pGA-modified UMEs, likely due to electrostatic repulsion between negatively charged groups in the films and the citrate capping agent on the Pt NPs. The important point is that collisions can be switched on and off using chemical interactions, and we believe this will form the basis for chemical sensing using the ECA approach.

■ EXPERIMENTAL SECTION

Chemicals and Materials. 11-Mercaptoundecanoic acid (95%), pGA (MW 100 000−150 000), L-ascorbic acid, citric acid, NaBH$_4$, and N$_2$H$_4$·H$_2$O were purchased from Sigma-Aldrich (St. Louis, MO). pLL (MW 30 000−70 000) was purchased from MP Biomedicals (Santa Ana, CA). Sodium citrate and sodium phosphate monohydrate were purchased from EM Science (Billerica, MA). H$_2$PtCl$_6$·6H$_2$O (99.9%) was purchased from Strem Chemicals (Newburyport, MA). Au-coated glass slides were purchased from Evaporated Metal Films (Ithaca, NY). Deionized water having a resistivity of 18.2 MΩ cm was used for all experiments (Milli-Q gradient water purification system, Millipore, Bedford, MA). All reagents were used as received. Experiments were conducted at room temperature (23 ± 2°C). Unless otherwise stated, the phosphate buffer was adjusted to pH 7.

Synthesis of Pt NPs. Pt NPs were synthesized using a previously reported seed-mediated procedure.[42] Briefly, 7.76 mL of a 0.2% (w/v) solution of H$_2$PtCl$_6$ was added to 100 mL of boiling H$_2$O. The solution was boiled for 1 min before addition of 2.37 mL of a solution containing 1% (w/v) sodium citrate and 0.05% (w/v) citric acid. After 30 s, 1.18 mL of a solution containing 0.08% (w/v) NaBH$_4$, 1% (w/v) sodium citrate, and 0.05% (w/v) citric acid was quickly injected. The solution was boiled for 10 min and subsequently cooled to ~25°C to yield 3.6 nm diameter Pt seed NPs. To synthesize larger NPs, 1.0 mL of the Pt seed solution was added to 29.0 mL of H$_2$O at ~25°C. While the solution was being stirred, 0.023 mL of a 0.40 M H$_2$PtCl$_6$ solution and 0.50 mL of a solution containing 1% sodium citrate and 1.25% L-ascorbic acid were added. The temperature of the solution was increased to the boiling point (100 °C) at a rate of 10 °C min^{-1}. The total reaction time was 30 min. Next, the solution was transferred to a 35 mm dialysis sack (12 000 Da MWCO, Sigma-Aldrich) and submerged in 4 L of H$_2$O for 24 h to remove excess salts. Lastly, the resulting NPs were characterized by transmission electron microscopy (TEM, FEI Tecnai Spirit BioTwin, 80 kV). The average particle diameter was 57 ± 10 nm. A representative TEM image, a histogram showing the NP size distribution, and a ζ-potential analysis are included in the Supporting Information (Figures S1 and S2).

Electrode Modification with MUA. Au UMEs (12.5 μm) were polished via wet sanding for 1 min. The UMEs were then immersed in piranha solution (1:3 30% H$_2$O$_2$/H$_2$SO$_4$) for 30 s and thoroughly rinsed with water. *Caution! Piranha solution can react violently with organic compounds and should be handled with care.* Next, electrochemical cleaning of the polished Au UME was performed by cycling the potential between −0.35 and 1.35 V versus Ag/AgCl (3.4 M KCl) for 25 cycles at 0.3 V s^{-1} (CH potentiostat model CH 700D, CH Instruments, Austin, TX). The electrodes were then rinsed with water and dried with a gentle stream of N$_2$. Lastly, the UMEs were immersed in a 10 mM ethanolic solution of MUA for 48 h and then rinsed with ethanol and water.

LbL Deposition of PEM Films. The first layer of pLL was deposited on a MUA-modified UME by incubating the electrode in a 0.5 M NaCl solution containing 2 mg mL^{-1} of pLL for 20 min, followed by rinsing with water. To deposit a second layer of pGA, the UME was incubated in a 0.5 M NaCl solution containing 2 mg mL^{-1} of pGA for 20 min. The deposition of the two oppositely charged polymers was repeated until the desired number of layers was obtained. The terminating polymer determined the net charge on the surface of the LbL-modified UMEs.[1,43] The thicknesses of the polymer layers were determined using spectroscopic ellipsometry (J.A. Woollam M2000 model, Lincoln, NE). Because of the small size of the electrodes, ellipsometric measurements were made on Au-coated glass slides.

Scheme 1
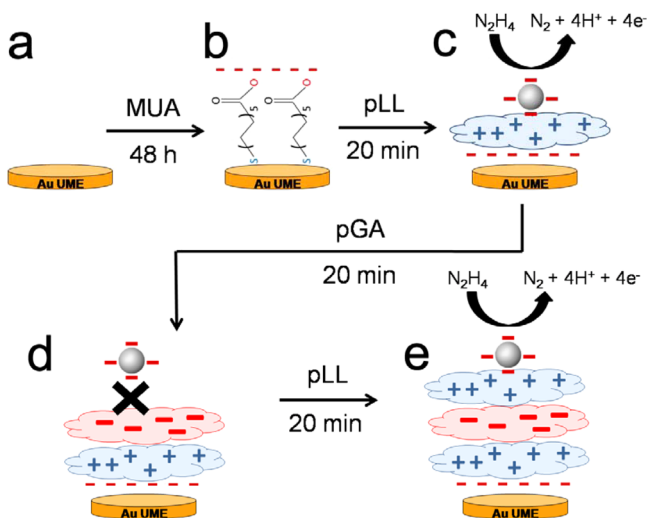
Electrochemistry. Au UMEs having a diameter of 12.5 μm were purchased from CH Instruments (Austin, TX). Cyclic voltammograms (CVs) and i−t curves were obtained in a two-electrode cell, contained within a Faraday cage, and using a Chem-Clamp voltammeter−amperometer (Dagan Corp., Minneapolis, MN) as the potentiostat. The applied voltage was generated by a PAR 175 Universal Function Generator (Princeton Applied Research, Oak Ridge, TN). The potentiostat and function generator were interfaced to a Dell Optiplex 380 computer through a PCI-6251 data acquisition board (National Instruments, Austin, TX) using a BNC-2090A analog breakout accessory (National Instruments, Austin, TX). The voltammetric and i−t measurements were performed using a custom LabView program (National Instruments), and the sampling time was 0.015 s. The Faraday cage was constructed from copper plate and mesh. Square wave voltammetry (SWV) was performed using a CH Instruments Model 650c potentiostat in a 3-electrode cell with a Pt wire serving as the counter electrode. SWV parameters: frequency, 390 Hz; incremental voltage, 5 mV; amplitude, 50 mV; and quiet time, 2 s. All potentials reported in this paper are referenced to a Ag/AgCl "leakless" reference electrode (3.4 M KCl, model 66-EE009, Dionex, Bannockburn, IL).

■ RESULTS AND DISCUSSION

UME Modification. The objective of this study is to better understand the nature of collisions between negatively charged Pt NPs and electrode surfaces modified with coatings having permanent positive and negative charges. The electrode modification process used to achieve the necessary experimental construct is outlined in Scheme 1 and described in detail in the Experimental Section. The insulating layer is formed by immersing a 12.5 μm diameter Au UME (Scheme 1a) in 10 mM MUA to yield a SAM (Scheme 1b). The terminal carboxylic acid group of the MUA monolayer is deprotonated and negatively charged at neutral pH (MUA surface pK_a, 5.7),[44] providing a foundation on which to deposit the first layer of positively charged pLL (Scheme 1c). Addition of a layer of negatively charged pGA reverses the net charge on the electrode surface (Scheme 1d), and the charge on the outermost layer can be reversed again by addition of a second pLL layer atop the pLL−pGA-modified UME (Scheme 1e).

SAM-Modified Au UMEs. Figure 1a presents CVs recorded at a naked Au UME (black trace) and the same UME after modification with MUA (red trace) in a solution containing 10 mM N₂H₄ and 50 mM PB (pH 7.0). In the presence of N₂H₄, the characteristic behavior of the N₂H₄ oxidation reaction on Au is apparent (onset potential, ~−0.15 V).[4] After modification with MUA, however, the decrease in the limiting current from ~80 to ~0.6 nA (inset, Figure 1a) indicates that the electrode surface is passivated. This decrease corresponds to a faradaic current suppression of ~99%. The onset potential for the oxidation reaction also shifts in the positive direction by ~200 mV, indicating increased resistance due to the presence of the SAM. Although a high level of passivation is achieved after deposition of MUA, the shape of the red CV remains sigmoidal (inset), indicating the presence of pinholes in the film.[45,46] The thickness of the SAM was determined to be ~1.7 nm using ellipsometry on Au-coated glass slides (used as surrogates for the UMEs, which are too small for ellipsometric measurements), which corresponds well to literature values.[47−49]

Square wave voltammetry (SWV) was used to estimate the surface coverage of the SAM (Figure 1b). The thiol desorption wave is centered at −1.2 V, which is consistent with previous findings.[50] The surface coverage can be calculated from the peak current in Figure 1b using eq 2.[51]
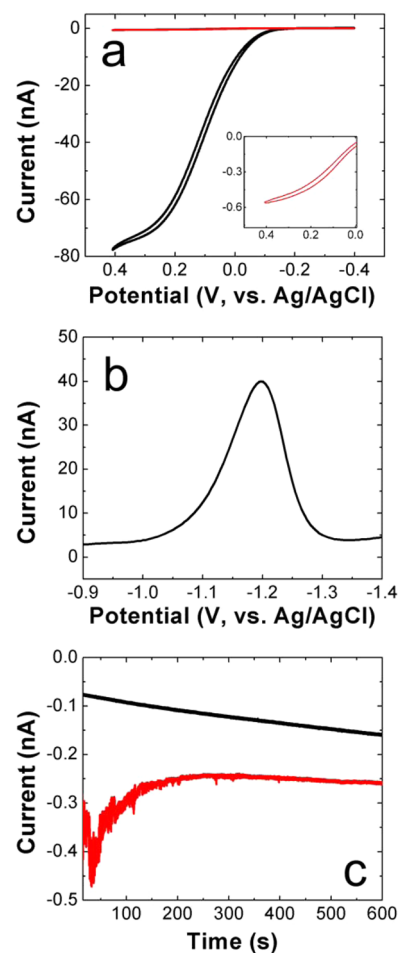

Figure 1. (a) CVs showing N₂H₄ oxidation at naked (black) and MUA-modified (red) 12.5 μm Au UMEs (no Pt NPs present). The inset shows an expanded view of the limiting current at the MUA-modified UME. CVs recorded at 50 mV s⁻¹; 10.0 mM N₂H₄ in 50 mM PB (pH 7). (b) Square wave voltammetry (SWV) characteristic of electrochemical removal of MUA from the electrode surface. SWV parameters: 0.5 M KOH, 390 Hz frequency, 5.0 mV step increments, and 50 mV amplitude. (c) i−t curves obtained at +400 mV for a MUA-modified UME recorded in a solution containing 10.0 mM N₂H₄ and 50 mM PB (pH 7) in the absence (black) and presence (red) of 2.5 pM Pt NPs.

$$i_p = 500A\alpha n^2 Faf\Delta E\Gamma \tag{2}$$

Here, i_p is the current amplitude, A the area of the electrode, α the transfer coefficient ($\alpha = $~0.5, values for thiol desorption on Au range from 0.4 to 0.84),[52,53] n the number of electrons ($n = $ 1), F Faraday's constant (96485 C mol⁻¹), a the square wave amplitude (0.05 V), f the applied frequency (390 Hz), ΔE the potential scan increment (5.0 mV), and Γ the surface coverage. On the basis of this analysis, $\Gamma = 6.1 \pm 2.0 \times 10^{-10}$ mol cm⁻², which is consistent with previous reports.[54,55]

After modification with MUA, collision experiments were performed in solutions containing 10 mM N₂H₄, 50 mM PB (pH 7), and Pt NP concentrations of 2.5, 5.0, 7.5, 10.0, and 12.5 pM. These experiments were carried out with the working electrode potential set to $E = 400$ mV because this value was determined to yield the largest current steps for the pLL and pLL−pGA−pLL systems discussed later. Figure 1c shows a representative i−t curve in the absence (black) and presence (red) of 2.5 pM Pt NPs. The current response in the absence of
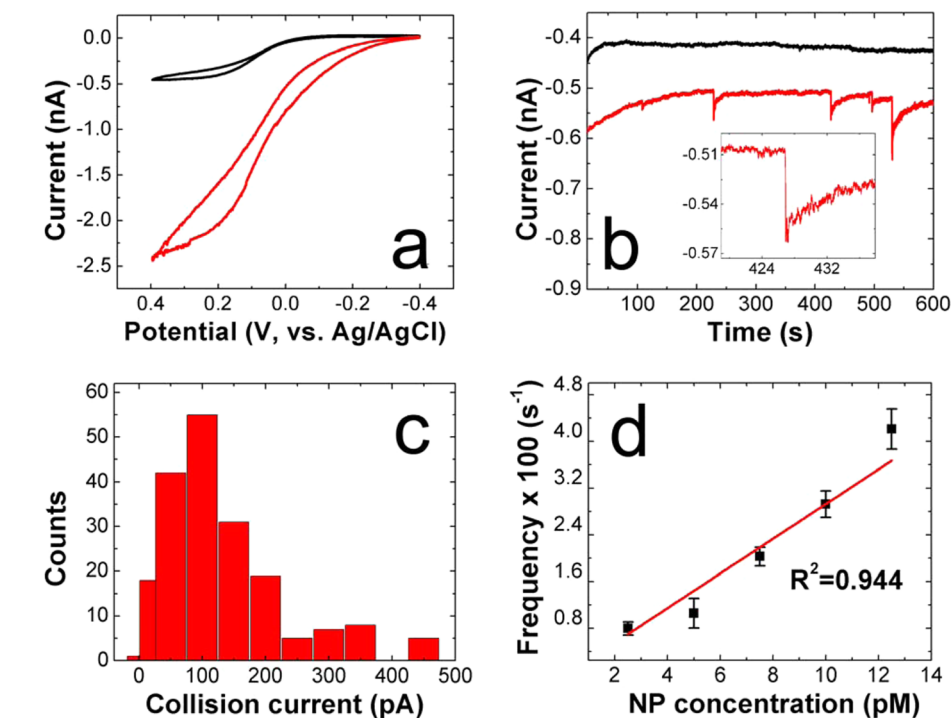
Figure 2. Electrochemical results obtained using a pLL-modified Au UME. For all experiments, the solution contained 10.0 mM N_2H_4 and 50 mM PB (pH 7). (a) CVs for a pLL-modified UME before (black) and after (red) a 600 s collision experiment using 5.0 pM Pt NPs. (b) $i-t$ curves recorded at +400 mV in the absence (black) and presence (red) of 5.0 pM Pt NPs. The inset shows an expanded view of a current transient exhibiting a step-like profile. (c) Histogram showing the distribution of current amplitudes for individual collisions. The average collision size is 140 $\pm$ 200 pA. (d) Plot of current–transient frequency (steps and peaks) as a function of the concentration of Pt NPs. The error bars represent the standard deviation of current signals obtained from three separate experiments at each concentration.

Pt NPs remains essentially constant at around −0.1 nA. Addition of Pt NPs to the system yields the appearance of small (<10 pA), spike-shaped current transients, indicating that the NPs may not be residing near the electrode long enough to stick to the exposed surface. This is in contrast to the result obtained for a naked Au UME, where NPs colliding and adsorbing to the surface yield step-like current transients.[4] The small amplitude of the transients is consistent with previous results obtained using an acid-terminated SAM.[6] Because the current transients for this system are very small, further analysis of their size and frequency were not conducted. Results similar to Figure 1c were also observed for Pt NP concentrations of 5.0, 7.5, 10.0, and 12.5 pM (Supporting Information, Figure S3).

Characterization of PEM Films. The thicknesses and permeability of PEM film layers depends on a number of parameters, including the molecular weight of the polymers, pH, deposition time, and the type and concentration of electrolyte used in the LbL deposition solutions.[56] Although the generally accepted model for films formed via LbL is that the charge of the deposited polyelectrolyte overcompensates the charge of the previous layer,[1] the Schlenoff group has recently reported that this charge reversal is likely asymmetrical.[57] High salt concentrations have been shown to stabilize alternately charged layers, resulting in thicker films;[58] therefore, 0.50 M NaCl was chosen for deposition of the LbL films used here. The growth of the LbL films on Au was monitored by ellipsometry up to $n = 10$, where n is an individual layer of either pLL or pGA (at $n = 10$, the terminating layer is pGA). The resulting total thicknesses are given in Figure S4 in the Supporting Information. The thicknesses of the pLL, pLL–

pGA, and pLL–pGA–pLL films used for collision studies were 0.5, 1.7, and 3.3 nm, respectively. These values do not include the MUA underlayer, which was previously found to be 1.7 nm in height. Notably, the thickness of each successive layer increases with n. This behavior is characteristic of the LbL process.[59] The total thickness at $n = 10$ (23.3 nm) is consistent with that of a similar pLL–pGA system studied by Corn and co-workers.[60]

Pt NP Collisions at pLL-Modified Au UMEs. Collision experiments were performed for each of the following three types of polymer thin films: pLL, pLL–pGA, and pLL–pGA–pLL. After modification via LbL deposition, each electrode was rinsed with H_2O and used immediately.

CVs were obtained before each experiment, and the average limiting current for N_2H_4 oxidation, determined using 15 independently prepared pLL-modified UMEs, was −0.4 $\pm$ 0.2 nA. UMEs yielding a limiting current higher than −0.7 nA were deemed too defective and not used for collision experiments. Figure 2a presents a typical CV (black trace) of a pLL-modified UME before introduction of Pt NPs. After obtaining the CV, a background $i-t$ curve was collected (Figure 2b, black trace). No current transients are observed, and the steady-state current is ∼−0.4 nA. After injection of 5.0 pM Pt NPs, however (Figure 2b, red trace), several large current steps characteristic of Pt NP collisions at naked Au electrodes are apparent.[4] These step-shaped transients (Figure 2b, inset) are likely due to electrostatic adsorption of the negatively charged Pt NPs (zeta potential (ζ), −59 mV, Figure S2 in the Supporting Information) to the positively charged pLL film. Recall that such large and easily discernible collision events were not observed for the MUA-only UMEs (Figure 1c), suggesting that
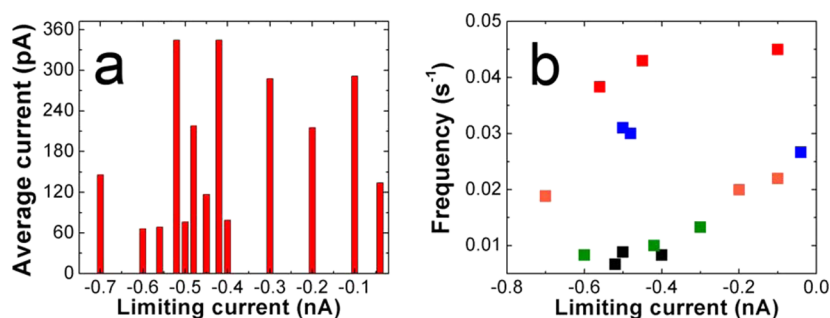
Figure 3. (a) Plot of average collision current for each pLL-modified Au UME versus the limiting current for N_2H_4 oxidation. The experiments were carried out in solutions containing 10.0 mM N_2H_4 and 50 mM PB (pH 7). The limiting current was determined from CVs obtained immediately after UME modification but prior to recording $i−t$ curves in the presence of Pt NPs. (b) Scatterplot of collision frequency versus the limiting current for N_2H_4 oxidation for each pLL-modified Au UME. The limiting current was determined from CVs obtained immediately after UME modification but prior to recording $i−t$ curves in the presence of Pt NPs. Three individual experiments are shown for each of five Pt NP concentrations: 2.5 (black), 5.0 (green), 7.5 (orange), 10.0 (blue), and 12.5 (red) pM.

collisions are not occurring at defect sites in the pLL film (more about defects later). In addition to the step-shaped current transients, spike-shaped collision signatures are also observed for the pLL films, especially at concentrations of Pt NPs greater than 7.5 pM (Figure S5 in the Supporting Information). These spike-shaped transients likely arise from rapid deactivation of the Pt NP surface, as has been previously shown by the Stevenson group for Hg electrodes.[22]

A histogram showing the collision current amplitudes for all of the pLL-modified UMEs (at all Pt NP concentrations) is shown in Figure 2c. Collision sizes larger than 500 pA, which accounted for <5% of all events, were excluded from this distribution as these large sizes are likely due to aggregated Pt NPs rather than individual particles. The average collision size across all of the pLL experiments performed is 140 ± 200 pA. Although the standard deviation for this average is large, it is comparable to the average collision size experimentally obtained at naked Au UMEs (185 ± 177 pA) for the same batch of Pt NPs. Note, however, that both of these values are smaller than the collision current of 613 pA calculated using eq 3,[4] which has previously been shown to provide reasonable agreement with experimental results for collisions using ∼4 nm NPs.[4]

$$I = 4\pi(\ln 2)nFDCr \qquad (3)$$

Here, D is the diffusion coefficient of the redox molecule (D for N_2H_4 is 6.4×10^{-6} cm^2 s^{-1})[26] and C is its concentration; r is the radius of the colliding NPs. We do not know why the currents calculated using this equation do not agree with the experimental results. One possibility is that the majority of observed collisions originate from a small subset of Pt NPs at the low end of the size distribution, and another possibility is that this empirical equation is simply not appropriate for the relatively large NPs (57 ± 10 nm) used in this study. Figure 2d presents collision frequencies over the full range of Pt NP concentrations examined. As has been found previously using naked Au UMEs, the frequency is linearly related to NP concentration.[13]

After each collision experiment, the UME was removed from solution, rinsed with H_2O, and then reimmersed in a fresh solution containing 10 mM N_2H_4 and 50 mM PB. Figure 2a (red trace) compares a CV of a pLL-modified UME after a collision experiment using 5.0 pM Pt NPs with the CV obtained prior to the collision experiments. The limiting current arising from N_2H_4 oxidation is much larger than it was

before the collision experiment (black trace). This observation is consistent with previous reports that adsorption of NPs onto LbL films leads to an enhanced current response compared to that of the passivating LbL film alone.[35,36,38] Accordingly, we conclude that the data in Figure 2a confirm that at least some of the colliding Pt NPs remain on the pLL surface and are active for electrocatalytic oxidation of N_2H_4. Further evidence of adsorbed Pt NPs on the pLL film comes from the negative shift of the onset potential for N_2H_4 oxidation, from ∼0 V to ∼−0.25 V. This is a consequence of the electrocatalytic properties of Pt relative to Au. Similar behavior is observed for CVs obtained after pLL-modified Au UMEs are immersed in a 128 pM Pt NP solution for 20 min (Figure S6 in the Supporting Information), which is known to result in electrostatic adsorption of Pt NPs.[35,37] Indeed, Figure S9 in the Supporting Information is an SEM image showing Pt NPs adsorbed onto the surface of a pLL-modified Au UME.

To reduce the likelihood of collisions occurring at defect sites within the LbL films, we used relatively large Pt NPs (57 ± 10 nm). Nevertheless, the question of whether these collisions are occurring on top of the polyelectrolyte film or within defects is both crucial and difficult to answer directly. We can, however, indirectly address this question in two ways. First, if collisions are occurring at defect sites, then a correlation should exist between the limiting current for N_2H_4 oxidation measured at pLL-modified UMEs (no Pt NPs) and the collision current amplitude.[45] That is, larger defects will permit direct collisions by larger Pt NPs (recall that because of aggregation, there is a broad distribution of Pt NPs in these experiments, Figure 2c), and this will in turn result in larger collision currents. Figure 3a is a histogram showing the average current due to Pt NP collisions versus the limiting current measured in the same solution (10 mM N_2H_4 plus 50 mM PB) and the same pLL-coated electrode prior to introduction of the Pt NPs. There is clearly no correlation between these parameters. For example, the UME with the highest limiting current (−0.7 nA), which should have the most defective pLL film, yields an average current amplitude value of ∼146 pA. However, this value is about half that observed at a more passivated UME (limiting current of −0.1 nA).

The second indirect evidence for collisions not occurring at defect sites within the pLL film is the following. A higher density of defect sites would provide more opportunities for direct collisions between Pt NPs and the naked Au surface. In other words, a positive correlation should exist between the
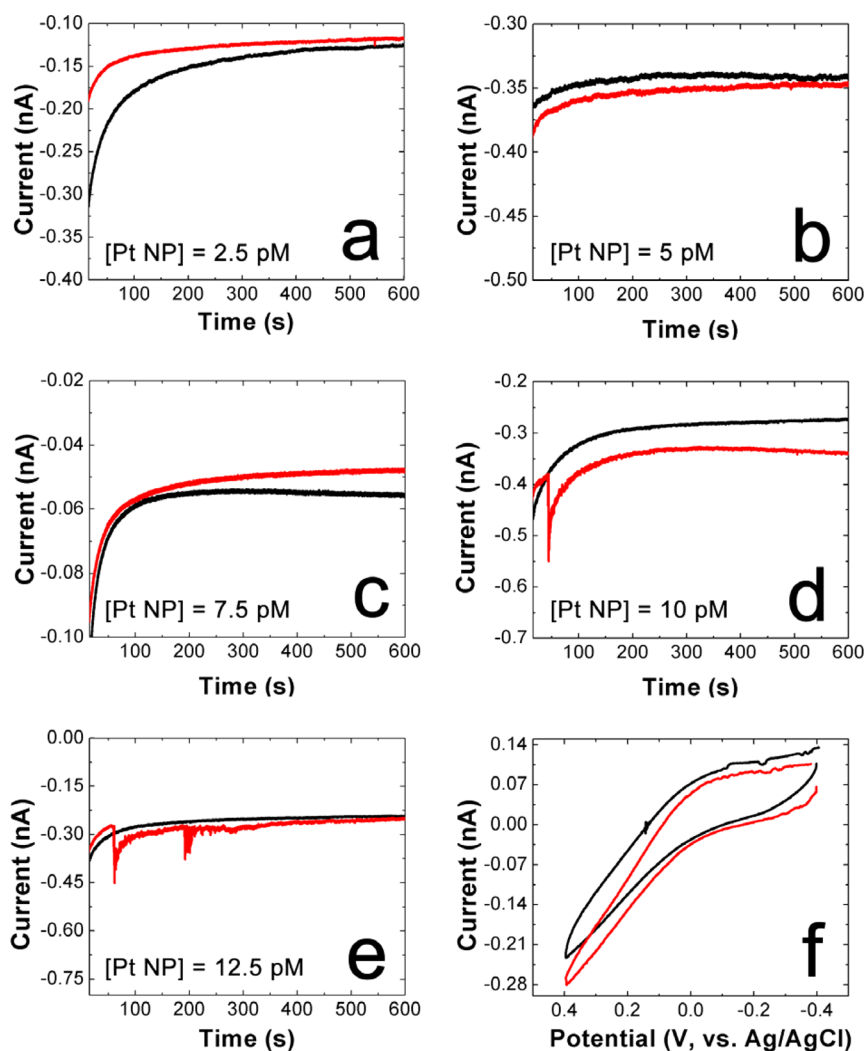
Figure 4. Electrochemical results obtained using a Au UME coated with a pLL–pGA PEM film. (a–e) i–t plots obtained at +400 mV in the absence (black) and presence (red) of Pt NPs at the indicated concentrations. (f) CVs obtained before (black) and after (red) a 600 s collision experiment using a 5.0 pM Pt NP solution. Scan rate: 50 mV s^{-1}. Solutions for all experiments contained 10.0 mM N$_2$H$_4$ and 50 mM PB (pH 7).

frequency of Pt NP collisions and the limiting current because of direct oxidation of N$_2$H$_4$ at the Au surface. As shown in Figure 3b, no such correlation is observed. For example, consider the results obtained using 5.0 pM Pt NPs (green data points). In this case, the UME with the highest limiting current (-0.6 nA) yields the lowest collision frequency (0.0083 s^{-1}).

The absence of correlations between the limiting current resulting from N$_2$H$_4$ oxidation at the Au UME and the current amplitude and collision frequency suggests that NP collisions are occurring at the solution–pLL interface rather than at naked regions of the Au surface.

Pt NP Collisions at MUA–pLL–pGA-modified Au UMEs. On the basis of the results observed using the negatively charged MUA SAM surface and the positively charged pLL surface, we surmised that addition of a negatively charged pGA polymer layer would suppress the collision amplitude and frequency of negatively charged Pt NPs. Results confirming this hypothesis are shown in Figure 4. For example, Figure 4a shows i–t traces in the absence (black) and presence (red) of 2.5 pM Pt NPs. In contrast to i–t traces for the pLL system (Figure S5a in the Supporting Information), no current transients are observed after addition of pGA, effectively shutting down electrocatalytic activity. This is likely due to electrostatic

repulsion between the outermost pGA film and the negatively charged Pt NPs.

Similar results are obtained for 5.0 and 7.5 pM Pt NP concentrations at pLL–pGA electrodes, as shown in Figure 4b,c. After addition of Pt NPs to the solution, no current transients arising from Pt NP collisions are observed. When the Pt NP concentration is 10 pM, one current transient is observed at ∼50 s. This may be due to a nonuniform distribution of the pGA film on top of the pLL layer. Although polyelectrolyte films formed by LbL deposition are generally thought to reverse the surface charge with each subsequent layer, polyelectrolytes are deposited as islands of varying thickness rather than as uniform layers.[58] Small exposed areas of the previous pLL layer may provide enough electrostatic attraction to allow a small number of current transients at this higher concentration. At the highest concentration of Pt NPs (12.5 pM), ∼4–5 collision events are observed per 600 s, but this number is much lower than that observed at pLL-modified UMEs (∼24 transients for the same Pt NP concentration and the same duration experiment).

Figure 4f shows CVs obtained before (black) and after (red) addition of 5.0 pM Pt NPs. The onset potential for N$_2$H$_4$ oxidation does not shift significantly, as was demonstrated for
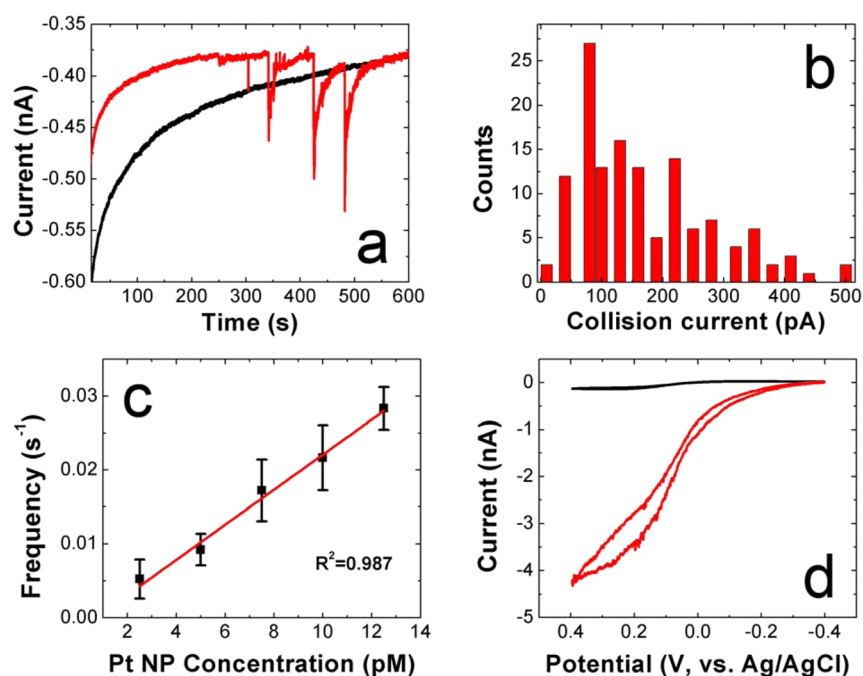
Figure 5. Electrochemical results obtained using a pLL−pGA−pLL-modified Au UME. For all experiments, the solution contained 10.0 mM N_2H_4 and 50 mM PB (pH 7). (a) i−t curves obtained at +400 mV recorded in the absence (black) and presence (red) of 5.0 pM Pt NPs. (b) Histogram showing the distribution of current amplitudes for individual collisions. The average collision amplitude is 157 ± 114 pA. (c) Plot of the frequency of current transients (steps and peaks) as a function of the concentration of Pt NPs. The error bars represent the standard deviation of current signals obtained from three separate experiments at each concentration. (d) CVs for a pLL−pGA−pLL-modified UME before (black) and after (red) a 600 s collision experiment using 5.0 pM Pt NPs.

the pLL system (Figure 2a), and there is no increase in current after addition of Pt NPs. This is evidence that an insignificant number of Pt NPs collide and adsorb onto the film during the i−t experiment. It is likely that the overall negative charge of pGA electrostatically repels the Pt NPs and hinders ECA on the Pt surface. To summarize, the addition of the pGA layer shuts off collisions between Pt NPs and the UME.

Pt NP Collisions at pLL−pGA−pLL-Modified Au UMEs. To confirm the importance of electrostatics in these types of collision experiments, and also to show that collisions can be detected through relatively thick LbL polymer films, we obtained i−t plots for Au UMEs modified with a second layer of positively charged pLL. Figure 5a shows representative i−t curves in the absence (black trace) and presence (red trace) of 5.0 pM Pt NPs for a MUA−pLL−pGA−pLL film. No current transients are observed in the absence of Pt NPs. In the presence of Pt NPs, however, collisions are observed, indicating reactivation of the UME. This reactivation of the electrode by addition of a second positively charged layer atop negatively charged pGA clearly points to the importance of electrostatics in these experiments. It also provides additional confidence that collisions are not occurring at pinholes in the LbL films because surely this thicker 3-layer film would contain fewer defects than the 2-layer, pGA-capped surface. Results similar to those shown in Figure 5a are provided in the Supporting Information for Pt NP concentrations ranging from 2.5−12.5 pM (Figure S7).

A histogram showing the distribution of collision amplitudes obtained using 15 independently prepared UMEs is shown in Figure 5b. The average collision size for this system is 157 ± 114 pA, which is similar to that obtained for Au UMEs modified with a single pLL layer (140 ± 200 pA). This means that within the context of the relatively large standard deviations, the collision currents are independent of film

thickness. This observation is consistent with reactivation trends observed by Gooding and co-workers.[61]

Figure 5c shows that the frequency of collisions is a linear function of NP concentration for the three-layer polymer film. An indication that electrons are tunneling from the Pt NP to the underlying electrode can be found in the CVs measured before and after collision experiments (Figure 5d). As for the MUA−pLL film (Figure 2a), an increase in the limiting current and a negative shift in the onset potential for N_2H_4 oxidation are observed. An analysis of limiting current, average collision size, and frequency of collisions similar to that carried out for the pLL-modified UMEs (Figure 3) can be found in the Supporting Information (Figure S8). As alluded to earlier, the absence of a correlation between these three variables suggests that collisions occur on top of the PEM films rather than at defects penetrating through the film to the underlying UME surface.

■ SUMMARY AND CONCLUSIONS

We have shown that collisions between Pt NPs and PEM films result in easily measurable currents. There are two interesting conclusions that can be drawn from this study. First, despite the thickness of the insulating PEM films (the 3-layer film, including the SAM layer, has an ellipsometric thickness of ∼5 nm) electrons are able to tunnel from the Pt NPs to the electrode resulting in electrocatalytic N_2H_4 oxidation at the PEM film−solution interface. These single-particle measurements are in accord with prior reports showing that the electrochemical activity of passive LbL films can be reactivated by adsorption of metallic NPs.[35,62−70] Second, it is possible to control the collisions by manipulating the net electrostatic charge present on the outer surface of the PEM thin film. These results, which demonstrate that chemistry can be used to

control ECA, set the stage for future sensing applications. Results from those experiments will be reported in due course.

■ ASSOCIATED CONTENT

ⓈSupporting Information

TEM images; NP size distributions; Nanosight particle analysis; $i-t$ curves for MUA-, pLL-, and pLL–pGA–pLL-modified UMEs; ellipsometry data; CVs for pLL-modified UMEs incubated in a Pt NP solution for 20 min; and plots of average collision current and collision frequency as a function of the N_2H_4 limiting current for the pLL–pGA–pLL film. This material is available free of charge via the Internet at http://pubs.acs.org.

■ AUTHOR INFORMATION

Corresponding Author
*E-mail: crooks@cm.utexas.edu. Tel.: 512-475-8674.
Notes
The authors declare no competing financial interest.

■ ACKNOWLEDGMENTS

■ REFERENCES

(1) Decher, G. Fuzzy Nanoassemblies: Toward Layered Polymeric Multicomposites. *Science* **1997**, *277*, 1232–1237.

(2) Hammond, P. T. Form and Function in Multilayer Assembly: New Applications at the Nanoscale. *Adv. Mater. (Weinheim, Ger.)* **2004**, *16*, 1271–1293.

(3) Xiao, X.; Bard, A. J. Observing Single Nanoparticle Collisions at an Ultramicroelectrode by Electrocatalytic Amplification. *J. Am. Chem. Soc.* **2007**, *129*, 9610–9612.

(4) Xiao, X.; Fan, F.-R. F.; Zhou, J.; Bard, A. J. Current Transients in Single Nanoparticle Collision Events. *J. Am. Chem. Soc.* **2008**, *130*, 16669–16677.

(5) Fan, F.-R. F.; Bard, A. J. Observing Single Nanoparticle Collisions by Electrogenerated Chemiluminescence Amplification. *Nano Lett.* **2008**, *8*, 1746–1749.

(6) Xiao, X.; Pan, S.; Jang, J. S.; Fan, F.-R. F.; Bard, A. J. Single Nanoparticle Electrocatalysis: Effect of Monolayers on Particle and Electrode on Electron Transfer. *J. Phys. Chem. C* **2009**, *113*, 14978–14982.

(7) Bard, A. J.; Zhou, H.; Kwon, S. J. Electrochemistry of Single Nanoparticles via Electrocatalytic Amplification. *Isr. J. Chem.* **2010**, *50*, 267–276.

(8) Zhou, H.; Fan, F.-R. F.; Bard, A. J. Observation of Discrete Au Nanoparticle Collisions by Electrocatalytic Amplification Using Pt Ultramicroelectrode Surface Modification. *J. Phys. Chem. Lett.* **2010**, *1*, 2671–2674.

(9) Kwon, S. J.; Bard, A. J. DNA Analysis by Application of Pt Nanoparticle Electrochemical Amplification with Single Label Response. *J. Am. Chem. Soc.* **2012**, *134*, 10777–10779.

(10) Zhou, H.; Park, J. H.; Fan, F.-R. F.; Bard, A. J. Observation of Single Metal Nanoparticle Collisions by Open Circuit (Mixed) Potential Changes at an Ultramicroelectrode. *J. Am. Chem. Soc.* **2012**, *134*, 13212–13215.

(11) Park, J. H.; Boika, A.; Park, H. S.; Lee, H. C.; Bard, A. J. Single Collision Events of Conductive Nanoparticles Driven by Migration. *J. Phys. Chem. C* **2013**, *117*, 6651–6657.

(12) Park, J. H.; Thorgaard, S. N.; Zhang, B.; Bard, A. J. Single Particle Detection by Area Amplification: Single Wall Carbon Nanotube Attachment to a Nanoelectrode. *J. Am. Chem. Soc.* **2013**, *135*, 5258–5261.

(13) Kwon, S. J.; Fan, F.-R. F.; Bard, A. J. Observing Iridium Oxide (IrOx) Single Nanoparticle Collisions at Ultramicroelectrodes. *J. Am. Chem. Soc.* **2010**, *132*, 13165–13167.

(14) Zhou, Y.-G.; Rees, N. V.; Compton, R. G. The Electrochemical Detection and Characterization of Silver Nanoparticles in Aqueous Solution. *Angew. Chem., Int. Ed.* **2011**, *50*, 4219–4221.

(15) Rees, N. V.; Zhou, Y.-G.; Compton, R. G. The Aggregation of Silver Nanoparticles in Aqueous Solution Investigated via Anodic Particle Coulometry. *ChemPhysChem* **2011**, *12*, 1645–1647.

(16) Zhou, Y.-G.; Rees, N. V.; Compton, R. G. Nanoparticle-Electrode Collision Processes: The Underpotential deposition of Thallium on Silver Nanoparticles in Aqueous Solution. *ChemPhysChem* **2011**, *12*, 2085–2087.

(17) Cutress, I. J.; Rees, N. V.; Zhou, Y.-G.; Compton, R. G. Nanoparticle-electrode collision processes: Investigating the contact time required for the diffusion-controlled monolayer underpotential deposition on impacting nanoparticles. *Chem. Phys. Lett.* **2011**, *514*, 58–61.

(18) Zhou, Y.-G.; Rees, N. V.; Compton, R. G. Nanoparticle-electrode collision processes: The electroplating of bulk cadmium on impacting silver nanoparticles. *Chem. Phys. Lett.* **2011**, *511*, 183–186.

(19) Rees, N. V.; Zhou, Y.-G.; Compton, R. G. Making contact: Charge transfer during particle-electrode collisions. *R. Soc. Chem. Adv.* **2012**, *2*, 379–384.

(20) Zhou, Y.-G.; Rees, N. V.; Compton, R. G. The electrochemical detection of tagged nanoparticles via particle-electrode collisions: Nanoelectroanalysis beyond immobilisation. *Chem. Commun. (Cambridge, U.K.)* **2012**, *48*, 2510–2512.

(21) Zhou, Y.-G.; Rees, N. V.; Pillay, J.; Tshikhudo, R.; Vilakazi, S.; Compton, R. G. Gold nanoparticles show electroactivity: Counting and sorting nanoparticles upon impact with electrodes. *Chem. Commun. (Cambridge, U.K.)* **2012**, *48*, 224–226.

(22) Dasari, R.; Walther, B.; Robinson, D. A.; Stevenson, K. J. Influence of the Redox Indicator Reaction on Single-Nanoparticle Collisions at Mercury- and Bismuth-Modified Pt Ultramicroelectrodes. *Langmuir* **2013**, *29*, 15100–15106.

(23) Fernando, A.; Parajuli, S.; Alpuche-Aviles, M. A. Observation of Individual Semiconducting Nanoparticle Collisions by Stochastic Photoelectrochemical Currents. *J. Am. Chem. Soc.* **2013**, *135*, 10894–10897.

(24) Sardesai, N. P.; Andreescu, D.; Andreescu, S. Electroanalytical Evaluation of Antioxidant Activity of Cerium Oxide Nanoparticles by Nanoparticle Collisions at Microelectrodes. *J. Am. Chem. Soc.* **2013**, *135*, 16770–16773.

(25) Kleijn, S. E. F.; Lai, S. C. S.; Miller, T. S.; Yanson, A. I.; Koper, M. T. M.; Unwin, P. R. Landing and Catalytic Characterization of Individual Nanoparticles on Electrode Surfaces. *J. Am. Chem. Soc.* **2012**, *134*, 18558–18561.

(26) Kleijn, S. E. F.; Serrano-Bou, B.; Yanson, A. I.; Koper, M. T. M. Influence of Hydrazine-Induced Aggregation on the Electrochemical Detection of Platinum Nanoparticles. *Langmuir* **2013**, *29*, 2054–2064.

(27) Wakerley, D.; Guell, A. G.; Hutton, L. A.; Miller, T. S.; Bard, A. J.; Macpherson, J. V. Boron doped diamond ultramicroelectrodes: A generic platform for sensing single nanoparticle electrocatalytic collisions. *Chem. Commun. (Cambridge, U.K.)* **2013**, *49*, 5657–5659.

(28) Kwon, S. J.; Zhou, H.; Fan, F.-R. F.; Vorobyev, V.; Zhang, B.; Bard, A. J. Stochastic electrochemistry with electrocatalytic nanoparticles at inert ultramicroelectrodes—Theory and experiments. *Phys. Chem. Chem. Phys.* **2011**, *13*, 5394–5402.

(29) Park, J. H.; Zhou, H.; Percival, S. J.; Zhang, B.; Fan, F.-R. F.; Bard, A. J. Open Circuit (Mixed) Potential Changes Upon Contact

Between Different Inert Electrodes-Size and Kinetic Effects. *Anal. Chem.* **2013**, *85*, 964−970.

(30) Guo, Z.; Percival, S. J.; Zhang, B. Chemically Resolved Transient Collision Events of Single Electrocatalytic Nanoparticles. *J. Am. Chem. Soc.* **2014**, *136*, 8879−8882.

(31) Alligrant, T. M.; Nettleton, E. G.; Crooks, R. M. Electrochemical detection of individual DNA hybridization events. *Lab Chip* **2013**, *13*, 349−354.

(32) Nuzzo, R. G.; Allara, D. L. Adsorption of bifunctional organic disulfides on gold surfaces. *J. Am. Chem. Soc.* **1983**, *105*, 4481−4483.

(33) Kim, J.; Kim, B.-K.; Cho, S. K.; Bard, A. J. Tunneling Ultramicroelectrode: Nanoelectrodes and Nanoparticle Collisions. *J. Am. Chem. Soc.* **2014**, *136*, 8173−8176.

(34) Chazalviel, J.-N.; Allongue, P. On the Origin of the Efficient Nanoparticle Mediated Electron Transfer across a Self-Assembled Monolayer. *J. Am. Chem. Soc.* **2011**, *133*, 762−764.

(35) Zhao, J.; Bradbury, C. R.; Fermín, D. J. Long-Range Electronic Communication between Metal Nanoparticles and Electrode Surfaces Separated by Polyelectrolyte Multilayer Films. *J. Phys. Chem. C* **2008**, *112*, 6832−6841.

(36) Dyne, J.; Lin, Y.-S.; Lai, L. M. H.; Ginges, J. Z.; Luais, E.; Peterson, J. R.; Goon, I. Y.; Amal, R.; Gooding, J. J. Some More Observations on the Unique Electrochemical Properties of Electrode-Monolayer-Nanoparticle Constructs. *ChemPhysChem* **2010**, *11*, 2807−2813.

(37) Liu, F.; Khan, K.; Liang, J.-H.; Yan, J.-W.; Wu, D.-Y.; Mao, B.-W.; Jensen, P. S.; Zhang, J.; Ulstrup, J. On the Hopping Efficiency of Nanoparticles in the Electron Transfer across Self-Assembled Monolayers. *ChemPhysChem* **2013**, *14*, 952−957.

(38) Barfidokht, A.; Ciampi, S.; Luais, E.; Darwish, N.; Gooding, J. J. Distance-Dependent Electron Transfer at Passivated Electrodes Decorated by Gold Nanoparticles. *Anal. Chem.* **2013**, *85*, 1073−1080.

(39) Su, L.; Gao, F.; Mao, L. Electrochemical Properties of Carbon Nanotube (CNT) Film Electrodes Prepared by Controllable Adsorption of CNTs onto an Alkanethiol Monolayer Self-Assembled on Gold Electrodes. *Anal. Chem.* **2006**, *78*, 2651−2657.

(40) Zhang, B.; Fan, L.; Zhong, H.; Liu, Y.; Chen, S. Graphene Nanoelectrodes: Fabrication and Size-Dependent Electrochemistry. *J. Am. Chem. Soc.* **2013**, *135*, 10073−10080.

(41) Kissling, G. P.; Bünzli, C.; Fermín, D. J. Tuning Electrochemical Rectification via Quantum Dot Assemblies. *J. Am. Chem. Soc.* **2010**, *132*, 16855−16861.

(42) Bigall, N. C.; Härtling, T.; Klose, M.; Simon, P.; Eng, L. M.; Eychmüller, A. Monodisperse Platinum Nanospheres with Adjustable Diameters from 10 to 100 nm: Synthesis and Distinct Optical Properties. *Nano Lett.* **2008**, *8*, 4588−4592.

(43) Ferriz-Mañas, M.; Schlenoff, J. B. Zeta Potential of Polyelectrolyte Multilayers Using the Spinning Disk Method. *Langmuir* **2014**, *30*, 8776−8783.

(44) Smalley, J. F.; Chalfant, K.; Feldberg, S. W.; Nahir, T. M.; Bowden, E. F. An Indirect Laser-Induced Temperature Jump Determination of the Surface pK_a of 11-Mercaptoundecanoic Acid Monolayers Self-Assembled on Gold. *J. Phys. Chem. B* **1999**, *103*, 1676−1685.

(45) Finklea, H. O.; Hanshew, D. D. Electron-transfer kinetics in organized thiol monolayers with attached pentaammine(pyridine) ruthenium redox centers. *J. Am. Chem. Soc.* **1992**, *114*, 3173−3181.

(46) Sheffer, M.; Vivier, V.; Mandler, D. Self-assembled monolayers on Au microelectrodes. *Electrochem. Commun.* **2007**, *9*, 2827−2832.

(47) Bain, C. D.; Troughton, E. B.; Tao, Y. T.; Evall, J.; Whitesides, G. M.; Nuzzo, R. G. Formation of monolayer films by the spontaneous assembly of organic thiols from solution onto gold. *J. Am. Chem. Soc.* **1989**, *111*, 321−335.

(48) Smith, E. L.; Alves, C. A.; Anderegg, J. W.; Porter, M. D.; Siperko, L. M. Deposition of metal overlayers at end-group-functionalized thiolate monolayers adsorbed at gold. 1. Surface and interfacial chemical characterization of deposited copper overlayers at carboxylic acid-terminated structures. *Langmuir* **1992**, *8*, 2707−2714.

(49) Balevicius, Z.; Ramanaviciene, A.; Baleviciute, I.; Makaraviciute, A.; Mikoliunaite, L.; Ramanavicius, A. Evaluation of intact- and fragmented-antibody based immunosensors by total internal reflection ellipsometry. *Sens. Actuators, B* **2011**, *160*, 555−562.

(50) Zhong, C.-J.; Porter, M. D. Fine structure in the voltammetric desorption curves of alkanethiolate monolayers chemisorbed at gold. *J. Electroanal. Chem.* **1997**, *425*, 147−153.

(51) Lovrić, M.; Komorsky-Lovrić, S.; Murray, R. W. Adsorption effects in square-wave voltammetry of totally irreversible redox reactions. *Electrochim. Acta* **1988**, *33*, 739−744.

(52) Aoki, K.; Kakiuchi, T. Probability theory of desorption kinetics of self-assembled alkanethiols stabilized with pair interaction. *J. Electroanal. Chem.* **1998**, *452*, 187−192.

(53) Vinokurov, I. A.; Morin, M.; Kankare, J. Mechanism of Reductive Desorption of Self-Assembled Monolayers on the Basis of Avrami Theorem and Diffusion. *J. Phys. Chem. B* **2000**, *104*, 5790−5796.

(54) Balasubramanian, S.; Revzin, A.; Simonian, A. Electrochemical Desorption of Proteins from Gold Electrode Surface. *Electroanalysis* **2006**, *18*, 1885−1892.

(55) Widrig, C. A.; Alves, C. A.; Porter, M. D. Scanning tunneling microscopy of ethanethiolate and *n*-octadecanethiolate monolayers spontaneously absorbed at gold surfaces. *J. Am. Chem. Soc.* **1991**, *113*, 2805−2810.

(56) Farhat, T. R.; Schlenoff, J. B. Doping-Controlled Ion Diffusion in Polyelectrolyte Multilayers: Mass Transport in Reluctant Exchangers. *J. Am. Chem. Soc.* **2003**, *125*, 4627−4636.

(57) Ghostine, R. A.; Markarian, M. Z.; Schlenoff, J. B. Asymmetric Growth in Polyelectrolyte Multilayers. *J. Am. Chem. Soc.* **2013**, *135*, 7636−7646.

(58) Schlenoff, J. B.; Ly, H.; Li, M. Charge and Mass Balance in Polyelectrolyte Multilayers. *J. Am. Chem. Soc.* **1998**, *120*, 7626−7634.

(59) Harris, J. J.; Bruening, M. L. Electrochemical and in Situ Ellipsometric Investigation of the Permeability and Stability of Layered Polyelectrolyte Films. *Langmuir* **2000**, *16*, 2006−2013.

(60) Cheng, Y.; Corn, R. M. Ultrathin Polypeptide Multilayer Films for the Fabrication of Model Liquid/Liquid Electrochemical Interfaces. *J. Phys. Chem. B* **1999**, *103*, 8726−8731.

(61) Shein, J. B.; Lai, L. M. H.; Eggers, P. K.; Paddon-Row, M. N.; Gooding, J. J. Formation of Efficient Electron Transfer Pathways by Adsorbing Gold Nanoparticles to Self-Assembled Monolayer Modified Electrodes. *Langmuir* **2009**, *25*, 11121−11128.

(62) Chirea, M.; García-Morales, V.; Manzanares, J. A.; Pereira, C.; Gulaboski, R.; Silva, F. Electrochemical Characterization of Poly-electrolyte/Gold Nanoparticle Multilayers Self-Assembled on Gold Electrodes. *J. Phys. Chem. B* **2005**, *109*, 21808−21817.

(63) Bethell, D.; Brust, M.; Schiffrin, D. J.; Kiely, C. From monolayers to nanostructured materials: An organic chemist's view of self-assembly. *J. Electroanal. Chem.* **1996**, *409*, 137−143.

(64) Lu, M.; Li, X. H.; Yu, B. Z.; Li, H. L. Electrochemical Behavior of Au Colloidal Electrode through Layer-by-Layer Self-Assembly. *J. Colloid Interface Sci.* **2002**, *248*, 376−382.

(65) Chirea, M.; Pereira, C. M.; Silva, F. Catalytic Effect of Gold Nanoparticles Self-Assembled in Multilayered Polyelectrolyte Films. *J. Phys. Chem. C* **2007**, *111*, 9255−9266.

(66) Santos, H. A.; Chirea, M.; García-Morales, V.; Silva, F.; Manzanares, J. A.; Kontturi, K. Electrochemical Study of Interfacial Composite Nanostructures: Polyelectrolyte/Gold Nanoparticle Multilayers Assembled on Phospholipid/Dextran Sulfate Monolayers at a Liquid−Liquid Interface. *J. Phys. Chem. B* **2005**, *109*, 20105−20114.

(67) Dowdy, C. E.; Leopold, M. C. Enhanced electrochemistry of nanoparticle-embedded polyelectrolyte films: Interfacial electronic coupling and distance dependence. *Thin Solid Films* **2010**, *519*, 790−796.

(68) Cortez, M. L.; Marmisollé, W.; Pallarola, D.; Pietrasanta, L. I.; Murgida, D. H.; Ceolín, M.; Azzaroni, O.; Battaglini, F. Effect of Gold Nanoparticles on the Structure and Electron-Transfer Characteristics of Glucose Oxidase Redox Polyelectrolyte-Surfactant Complexes. *Chem.—Eur. J.* **2014**, *20*, 13366−13374.

(69) Schmidt, A. R.; Nguyen, N. D. T.; Leopold, M. C. Nanoparticle Film Assemblies as Platforms for Electrochemical Biosensing-Factors Affecting the Amperometric Signal Enhancement of Hydrogen Peroxide. *Langmuir* **2013**, *29*, 4574−4583.

(70) Ou, C.; Yuan, R.; Chai, Y.; Tang, M.; Chai, R.; He, X. A novel amperometric immunosensor based on layer-by-layer assembly of gold nanoparticles−multi-walled carbon nanotubes-thionine multilayer films on polyelectrolyte surface. *Anal. Chim. Acta* **2007**, *603*, 205−213.